Improved Thermal Cyclability of Tertiary Battery Made of Prussian Blue Analogues

Izumi Takahara[a], Assistant Prof. Takayuki Shibata*[a], Yuya Fukuzumi[b], and Prof. Yutaka Moritomo*[c]

Abstract: Tertiary battery is charged by the environmental heat, not by the electric energy, by using the difference ($\Delta\alpha$) in the thermal coefficient (α = dV/dT) of redox potential (V) between the anode and cathode materials. The thermal cyclability is not good in the prototypical $Na_xCo[Fe(CN)_6]_{0.71}$ (NCF71)/$Na_xCo[Fe(CN)_6]_{0.90}$ (NCF90) tertiary battery. Here, we significantly improved the thermal cyclability of the tertiary battery with using Ni-substituted $Na_xNi[Fe(CN)_6]_{0.68}$ (NNF68). The Ni-substituted NNF68/NCF90 tertiary battery shows good thermal cyclability: both the cell voltage and capacity essentially unchanged up to the 10th thermal cycles.

Introduction

An innovative energy harvesting technology, which converts waste heat near room temperature and/or human body heat to electric energy at low cost and high efficiency, is required to realize a smart society. Recently, several researchers[1] reported that the environmental heat can put a battery in a charged state by using the difference ($\Delta\alpha$) in the thermal coefficient (α = dV/dT) of the redox potential (V) between the anode and cathode materials. Hereafter, we call the battery "tertiary battery", because it is charged by the environmental heat, not by the electric energy. The tertiary battery generates electric energy in the thermal cycle between low (T_L) and high (T_H) temperatures. In the warming process, the battery shows the cell voltage (V_{cell}) of $\Delta\alpha\Delta T$ (ΔT = $T_H - T_L$) and the accumulated electric energy can be extracted by discharging the cell at T_H. Similarly, the cooling process induces V_{cell} (= - $\Delta\alpha$ ΔT). From a thermodynamically point of view, α is nothing but $\Delta S/e$, where e and ΔS are the elementary charge (> 0) and the differences in entropy of the system between reduced and oxidized states. In a battery system, ΔS consists of components of electrode and that of electrolyte, because the redox process accompanies ion exchange between them. [2]

PBAs, denoted as $Na_xM[Fe(CN)_6]_y$ (M is a transition metal), show three-dimensional (3D) cyano-bridged transition metal network, -M-NC-Fe-CN-M-, with cubic nanopores of 5 Å on each side.[3] Most of PBAs have face-centered cubic ($Fm\bar{3}m$; Z = 4) or trigonal ($R\bar{3}m$; Z = 3) structures.[4] The reduction/oxidization process of the network causes intercalation/deintercalation of Na^+ into/from the nanopores. Consequently, PBAs are promising not only as cathode materials for the secondary batteries[5] but also as tertiary battery materials. In addition, PBA exhibits reversible redox reaction even in aqueous solution,[6] which is incombustible and environmentally-friendly. This feature is significant when the materials are used in tertiary batteries, because they do not need wide potential window like the secondary batteries. Shibata *et al.*[1d)] fabricated a tertiary battery made of two kinds of cobalt Prussian blue analogues (PBA) with different α, *i.e.*, $Na_xCo[Fe(CN)_6]_{0.71}$ (NCF71) and $Na_xCo[Fe(CN)_6]_{0.90}$ (NCF90), and aqueous electrolyte. The NCF71/NCF90 tertiary battery produces electric energy with thermal efficiency (η) of 1.0 % between T_L (= 295 K) and T_H (= 323 K). The thermal cyclability of the NCF71/NCF90 tertiary battery, however, is not good. To put the tertiary battery into practical use, improvement of the thermal cycle cyclability is indispensable.

In this paper, we compared the thermal cyclability between the prototypical NCF71/NCF90 tertiary battery and Ni-substituted $Na_xNi[Fe(CN)_6]_{0.68}$ (NNF68)/NCF90 tertiary battery. We found that the thermal cyclability significantly improved in the Ni-substituted tertiary battery. In the NNF68/NCF90 tertiary battery, both the cell voltage [V_{cell}(40K)] at ΔT (= $T_H - T_L$) = 40 K and capacity (Q) essentially unchanged up to the 10th thermal cycles.

Results and Discussion

We first investigate the discharge curves of the NCF90, NCF71, and NNF68 films in aqueous solution containing 17 mol/kg $NaClO_4$ with 8.7 % addition of 0.1 mol/L HCl. **Figure 1** (a), (b), and (c) show the discharge curves of the NCF90, NCF71, and NNF68 films, respectively. In the (a) NCF90 film, the curve shows two plateaus near 1.0 and 0.55 V vs. Ag/AgCl, whose feature is the same as that obtained in propylene carbonate (PC) containing 1M $NaClO_4$.[7] Therefore, the redox site at lower (higher) is Co^{3+}/Co^{2+} (Fe^{3+}/Fe^{2+}). In the (b) NCF71 film, the curve shows single plateaus near 0.55 V vs Ag/AgCl, which is ascribed to the redox reaction of Fe^{3+}/Fe^{2+}[8]. Similarly, the curve of in the (c) NNF68 film shows single plateaus near 0.4 V vs. Ag/AgCl, which

[a] I. Takahara and Assistant Prof. T. Shibata
Gumma College
National Institute of Technology
Maebashi, Gumma, 371-8530, Japan
shibata@nat.gunma-ct.ac.jp
[b] Y. Fukuzumi (JSPS Research fellow)
Graduate School of Pure & Applied Science
University of Tsukuba
Tsukuba, 305-8571, Japan
[b] Prof. Y. Moritomo
Graduate School of Pure & Applied Science
Faculty of Pure & Applied Science
Tsukuba Research Centre for Energy Materials Science (TREMS)
University of Tsukuba
Tsukuba, 305-8571, Japan
moritomo.yutaka.gf@u.tsukuba.ac.jp

Supporting information for this article is given via a link at the end of the document.

is ascribed to the redox reaction of Fe^{3+}/Fe^{2+}[9]. Importantly, the redox potentials (V) of the lower plateaus are nearly the same among the three films, which is necessary condition to fabricate tertiary battery.

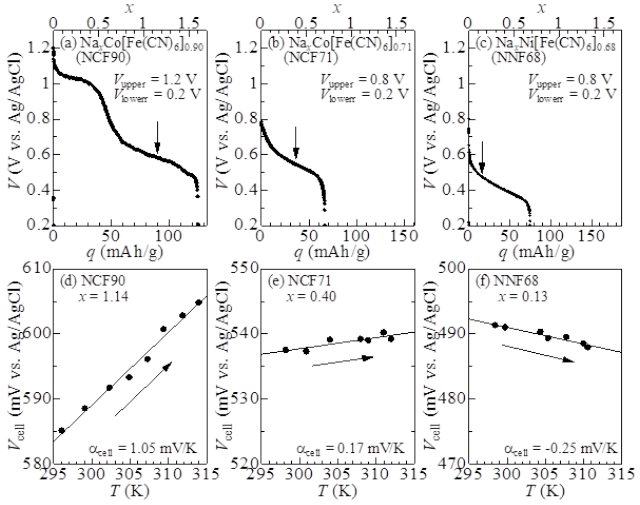

Figure 1. Discharge curves of (a) $Na_xCo[Fe(CN)_6]_{0.9}$ (NCF90), (b) $Na_xCo[Fe(CN)_6]_{0.71}$ (NCF71), and (c) $Na_xNi[Fe(CN)_6]_{0.68}$ (NNF68) films. The current density was 10 μA/cm^2. The cell voltage (V_{cell}) of the (d) NCF90, (e) NCF71, and (f) NNF68 films against temperature (T) in the warming run. Solid straight lines are results of the least-squares fitting. Arrows in (a), (b), and (c) represent the x values, where the T-dependences of V were measured.

The temperature coefficient (α) of V is expressed as $\alpha = \alpha_{cell} - \alpha_{ref}$, where α_{cell} and α_{ref} are the coefficient of the cell and referential electrode, respectively. In the present work, the coefficient of the referential electrode (Ag/AgCl standard electrode) was - 0.48 mV/K[10]. **Figure 1** (d), (e), and (f) show the cell voltage (V_{cell}) of the three films against T in the warming run. The α_{cell} values were evaluated by least-squares fittings, as indicated by solid straight lines. With use of the relation that $\alpha = \alpha_{cell}$ + 0.48 mV/K, we obtained α_{NCF90} = 1.53 mV/K for NCF90 (x = 1.14), α_{NCF71} = 0.65 mV/K for NCF71 (x = 0.40), and α_{NNF68} = 0.23 mV/K for NNF68 (x = 0.13). Strictly speaking, α depends on both the electrode and electrolyte, because the process accompanies exchange of Na^+ between them. In the oxidized state, Na^+ dissolves in the electrolyte to form a solvated state, whose entropy strongly depends on the electrolyte. We note that the electrolyte (aqueous solution containing 17 mol/kg $NaClO_4$ with 8.7 % addition of 0.1 mol/L HCl) is the same for the three PBA cells. Then, the electrolyte component of α is the same for the three PBAs and cannot explain material dependence of α.

We emphasize that the coefficient (α_{NCF90} = 1.53 mV/K) of the NCF90 film is much higher than those in the NCF71 (α_{NCF71} = 0.65 mV/K) and NNF68 (α_{NNF68} = 0.23 mV/K) films. The enhanced α in the NCF90 film can be ascribed to the difference in the redox site; the redox site of NCF90 is Co while those of NCF71 and NNF68 are Fe. From a thermodynamically point of view, α is equivalent to $(S_{3d}^{di}-S_{3d}^{tri})/e$, where S_{3d}^{di} and S_{3d}^{tri} are the 3d-electron configuration entropy of the redox site in the divalent and trivalent states, respectively. S_{3d} is expressed as $k_B \ln W$, where k_B and W (= $N_{spin}N_{orbital}$, where N_{spin} and $N_{orbital}$ are spin and orbital degrees of freedom, respectively) is the Boltzmann constant and number of degenerated electronic configuration. In PBAs, the oxidization process of Co^{2+} causes spin state transition from high-spin (Co^{2+}; $t_{2g}^5e_g^2$) to low-spin (Co^{3+}; t_{2g}^6) states while the oxidization process of Fe^{2+} changes the electronic configuration from low-spin (Fe^{2+}; t_{2g}^5) to low-spin (Fe^{3+}; t_{2g}^6) states. N_{spin} is expressed as $2S + 1$, where S is the total spin quantum number. $N_{orbital}$ = 3 in the $t_{2g}^5e_g^2$ and t_{2g}^5 configurations while $N_{orbital}$ = 1 in the t_{2g}^6 configuration. The redox process of Co^{2+}/Co^{3+} contributes to α by 0.21 mV/K[11] while that of Fe^{2+}/Fe^{3+} contributes to α by - 0.15 mV/K[11]. Thus, 3d-electron configuration entropy of the redox site qualitatively explains why α in NCF90 is larger than those in NCF71 and NCF68.

Figure 2 shows the thermal cycle properties of the Ni-substituted NNF68/NCF90 tertiary battery at ΔT (= T_H - T_L) = 40 K. At the 1st cycle (black) in the (a) warming process, V_{cell} linearly increases with the increase in T at a rate of 1.1 mV/K. The rate is comparable to α_{NCF90} - α_{NNF68} (=1.3 mV/K). At T_H, V_{cell} becomes 40 mV. In the (b) discharge process at T_H, V_{cell} linearly decreases to 0 V with the charge (q). The capacity (Q) is 10 mAh/g, which is 8.2% of the capacity of NCF90. In the (c) cooling process, V_{cell} linearly decreases with the decrease in T at a rate of 1.1 mV/K. At T_L, V_{cell} becomes - 45 mV. In the (d) discharge process at T_L, Q is 12.5 mAh/g. The thermal cyclability of the NF68/NCF90 tertiary battery is good; the properties at the 5th (red) and 10th (blue) cycles are essentially the same as that of the 1st cycle (black).

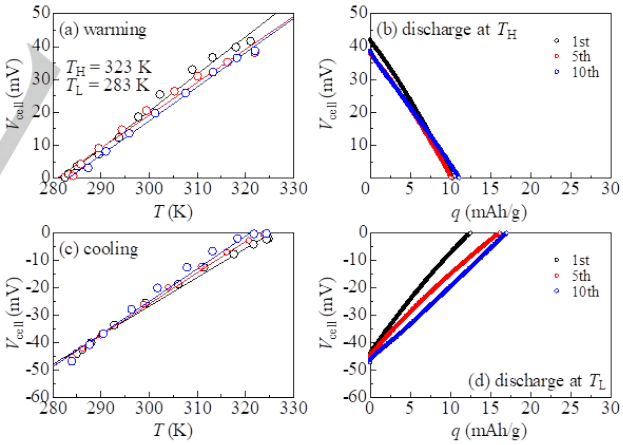

Figure 2. (a) Cell voltage (V_{cell}) of the NNF68/NCF90 tertiary battery against temperature (T) measured in the warming run under the open circuit condition at the 1st, 5th, and 10th cycles. Solid straight lines are results of the least-squares fitting. (b) Discharge curves at T_H (=323 K) against charge (q). (c) V_{cell} against T measured in the cooling run under the open circuit condition. Solid straight lines are results of the least-squares fittings. (d) Discharge curves at T_L (= 283 K).

It is rather curious that Q at T_L [Fig.2(d)] is slightly larger than that at T_H [(b)]. **Figure 3** (a) schematically shows the thermal cycle of tertiary battery in the V_{cell} – q plane. Q is expressed as $Q = -\Delta V_{cell}/(dV_{cell}/dq)$[1f)], where ΔV_{cell} (= $\alpha_{cell}\Delta T$) is the thermally induced

cell voltage. Note that the sign of ΔV_{cell}, and hence Q, reverses between T_H and T_L. If V_{cell} is stable against time [(a)], Q at T_L should be the same as that at T_H. If V_{cell} is unstable and changes by δ (< 0) [(b)], apparent asymmetry of Q appears between T_H and T_L. In the initial warming process, ΔV_{cell} (>0) and Q is the same as those in the stable case. In the next cooling process, ΔV_{cell} (< 0) effectively increases by δ. Then, Q at T_L increases by $\delta/(dV_{cell}/dq)$. We note that the enhancement of Q is observed only at T_L because the signs at T_H are opposite between ΔV_{cell} (> 0) and δ (< 0). Even the voltage fluctuations in the order of several millivolts causes asymmetry of Q because ΔV_{cell} is several tens of millivolts. Consistently with these arguments, $|\Delta V_{cell}|$ in the cooling process [**Figure 2** (c)] is slightly larger than that in the warming process [**Figure 2** (a)]. The asymmetry of Q causes gradual variation in the Na concentration (x) with cycle.

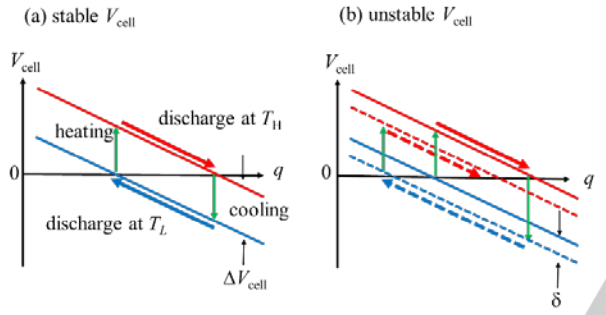

Figure 3 Thermal cycles of tertiary battery with (a) stable and (b) unstable cell voltage (V_{cell}.) ΔV_{cell} (= $\alpha_{cell}\Delta T$) and q are the thermally induced cell voltage and charge. δ is temporal variation of V_{cell}.

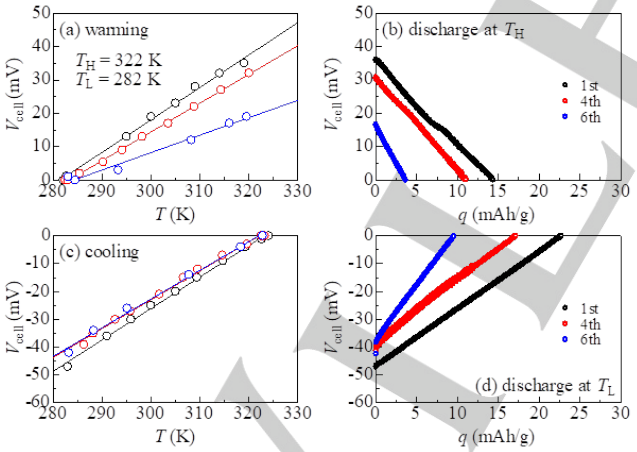

Figure 4. (a) Cell voltage (V_{cell}) of the NCF71/NCF90 cell against T measured in the warming run under the open circuit condition at the 1st, 4th, and 6th cycles. Solid straight lines are results of the least-squares fitting. (b) Discharge curves at T_H (=322 K) against charge (q). (c) V_{cell} against T measured in the warming run under the open circuit condition. Solid straight lines are results of the least-squares fittings. (d) Discharge curves at T_L (= 282 K).

The good thermal cyclability observed in the Ni-substituted NNF68/NCF90 tertiary battery is in sharp contrast with the poor thermal cyclability of the NCF71/NCF90 tertiary battery. **Figure 4** shows the thermal cycle properties of the NCF71/NCF90 tertiary battery at ΔT = 40 K. In the (a) warming process at the 1st cycle (black), V_{cell} linearly increases with the increase in T at a rate of 1.0 mV/K. The rate is comparable to α_{NCF90} - α_{NNF68} (= 0.9 mV/K). The rate, however, steeply decreases with cycle number; 0.8mV/K at the 4th cycle (red) and 0.4 mV/K at the 6th cycle (blue). In the (b) discharge at T_H at the 1st cycle (black), Q is 14.3 mAh/g, which is 11.4% of the capacity of NCF90. Q, however, steeply decreases with cycle number; 11.0 mAh/g at the 4th cycle (red) and 3.6 mAh/g at the 6th cycle (blue).

Figure 5 shows (a) Q and (b) cell voltage [V_{cell} (40K)] at ΔT = 40 K against cycle number. In the NNF68/NCF90 tertiary battery (open red circles), both Q and V_{cell} (40K) essentially unchanged up to the 10th thermal cycle. In the NCF71/NCF90 tertiary battery (filled blue circles), however, Q steeply decreases with cycle number at a rate of - 11 %/cycle. In addition, V_{cell} (40K) decreases with cycle number at a rate of - 7 %/cycle. The substitution of Ni for Co in the NCF71 film significantly improves the deteriorations of the NCF71/NCF90 tertiary battery. In other words, the bad thermal cyclability of the NCF71/NCF90 cell is originated in the NCF71 film, not in the NCF90 film.

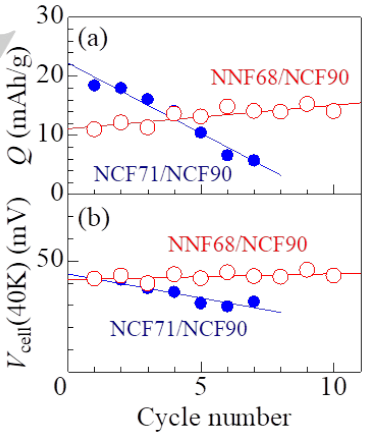

Figure 5. (a) Capacity (Q) and (b) cell voltage [V_{cell} (40K)] at ΔT = 40 K in the NNF68/NCF90 (open red circles) and NCF71/NCF90 (filled blue circles) tertiary batteries against cycle number. Average values of the warming and cooling runs are plotted. Solid straight lines are results of the least-squares fittings.

Figure 6 shows discharge curves of the (a) NCF71 and (b) NNF68 films against cycle number at T_L (= 283 K; blue) and T_H (= 323 K; red), respectively. At T_L, no trace of the capacity deterioration was observed in both the films up to the 10th cycle. At T_H, however, serious capacity deterioration was observed in the NCF71 film [**Figure 5** (a)]. The capacity at the 2nd (3rd) cycle is 57 % (12 %) of that at the 1st cycle. Such a capacity deterioration of the NCF71 film causes the poor thermal cyclability of the NCF71/NCF90 tertiary battery. The origin of the capacity deterioration is perhaps the cracks formation in the particles, since the NCF71 films sometimes peeled off during the washing

after the cyclability test. The substitution of Ni for Co significantly improves the capacity deterioration [**Figure 6** (b)] and causes the good thermal cyclability of the NNF68/NCF90 tertiary battery (**Figure 5**). Similarly, Xie *et al.* [5i)] reported that cyclability of $Na_2Co_{1-z}Ni_z[Fe(CN)_6]$ as cathode material for the sodium ion secondary battery in ethylene carbonate (EC) / diethyl carbonate (DEC) containing 1M $NaPF_6$ becomes better with the increase in the Ni concentration (z). The capacities at the 100th cycle are 49.2 %, 89.5 %, and 91.7 % of those at the first cycle at z = 0.0, 0.5, and 1.0, respectively.

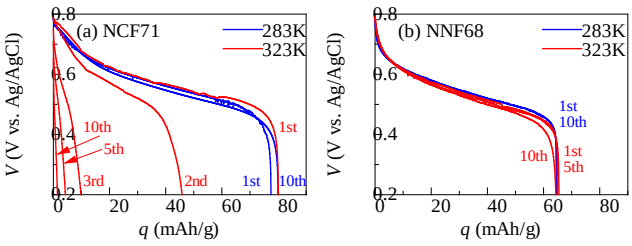

Figure 6. Discharge curves of the (a) NCF71 and (b) NNF68 films up to the 10th cycle. The blue and red curves represent the data measured at T_L (= 283 K) and T_H (= 323 K), respectively. The current density was 10 μA/cm^2.

Table 1. Crystallinity, density of $[Fe(CN)_6]$ deficiency, and unit cell size (a) of the NCF71, NCF90, and NNF68 films.

Film	crystallinity	density of $[Fe(CN)_6]$ deficiency	a (nm)
NCF71	High	29%	~ 1.03[8]
NCF90	High	10%	< 1.02[7]
NNF68	Low	68%	~ 1.02[9]

Here, we consider the necessary conditions and possible mechanism for the crack formation in PBA particles. Figure S1 shows scanning electron microscope (SEM) image of the NCF71. NCF90, and NNF68 films. The NCF90 and NCF71 films consists of crystalline particles about 100 nm in diameter, while the NNF68 film consists of granular particles with low crystallinity. Figure S2 shows X-ray diffraction pattern (XRD) of the NCF71, NCF90, and NNF68 films. The diffraction peaks of the NNF68 film is much broader than those of the NCF71 and NCF90 films, indicating smaller domain size (~ 20 – 70 nm) in the NNF68 film. On the other hand, the unit cell size (a) of NCF90[7] and NNF68[9] is less than 1.02 nm in the entire region of x, and is smaller than that (~ 1.03 nm[8] in the entire region of x of NCF71. We summarized In **Table 1** particle crystallinity and a of the NCF71, NCF90, and NNF68 films, together with the density of $[Fe(CN)_6]$ deficiencies. The NCF71 film, whose cyclability is bad due to crack formation, has higher crystallinity, higher-density of the $[Fe(CN)_6]$ deficiency, and larger unit cell size. It is reasonable that the high crystallinity makes the crack formation easier. In addition, the high-density Fe deficiencies and large unit cell size causes the highly porous structure, which is amenable for the crack formation during the chare/discharge process at T_H. On the other hands, the NNF68 film with lower crystallinity and smaller unit cell size is robust against the crack formation during the chare/discharge process.

Conclusions

We compared the thermal cyclability between the prototypical NCF71/NCF90 tertiary battery and Ni-substituted NNF68/NCF90 tertiary battery. We found that the thermal cyclability significantly improved in the Ni-substituted tertiary battery. Both the cell voltage [V_{cell}(40K)] at ΔT = 40 K and capacity (Q) essentially unchanged up to the 10th thermal cycles. Our experiment reveals that the poor cyclability of the NCF71 film at T_H (= 323 K) is responsible for the poor thermal cyclability of the NCF71/NCF90 tertiary battery. Present work indicates that tertiary batteries are one of the promising energy harvesting devices.

Supporting Information and Summary

Scanning Electron microscope (SEM) images and X-ray diffraction (XRD) patterns of the as-grown NCF71, BCF90, and NNF68 films are shown.

Acknowledgements

This work was supported by JSPS KAKENHI (Grant Number JP17H01137 and 19J12284), the Japan Prize Foundation, and a joint research with Focus Systems Corporation. The elementary analyses were performed at the Chemical Analysis Division, Research Facility Center for Science and Engineering, University of Tsukuba.

I. Takahara fabricated the NNF68/NCF90 and NCF71/NCF90 tertiary batteries and measured thermal cyclability on each batteris. Y. Fukuzumi characterized the PBA films. T. Shibata and Y. Moritomo planed the research and wrote the manuscript.

Keywords: energy harvesting • Prussian blue analogues • substitution effect • tertiary battery • thermal cyclability

[1] a) S. W. Lee, Y. Yang, H.-W. Lee, H. Ghasemi, D. Kraemer, G. Chen, Y. Cui, *Nat. Commun.* **2014**, *5*, 3942, b) Y. Yang, S. W. Lee, H. Ghasemi, J. Loomis, X. Li, D. Kraemer, G. Zheng, Y. Cui, G. Chen, *PNAS* **2014**, *111*, 17011-17116, c) J. Wang, S.-P. Feng., Y. Yang, N. Y. Hau, M. Munro, E. Ferreira-Yang, G. Chen, *Nano Lett.* **2015**, *15*, 5784-5790, d) T. Shibata, Y. Fukuzumi, W. Kobayashi, Y. Moritomo, *Appl. Phys. Express* **2018**, *11*, 017101, e) Y. Fukuzumi, K. Amaha, H. Niwa, W. Kobayashi, Y. Moritomo, *Energy Technol.* **2018**, *6*, 1865-1870, f) T. Shibata, Y. Fukuzumi, Y. Moritomo, *Sci. Reps.* **2018**, *8*, 14784

[2] a) Y. Fukuzumi, Y. Hinuma, Y. Moritomo, J. Phys. Soc. Jpn. **2018**, *87*, 055001, b) Y. Fukuzumi, Y. Hinuma, Y. Moritomo, *AIP Adv.*, **2018** *6*, 065021.

[3] a) H. J. Buser, D. Schwarzenbach, W. Petter, A. Ludi, *Inorg. Chem.* **1977**, *16*, 2704-2710, b) F. Herren, P. Fischer, A. Ludi, W. Halg, *Inorg. Chem.* **1980**, *19*, 956-959.

[4] H. Niwa, W. Kobayashi, T. Shibata, H. Nitani, Y. Moritomo, *Sci. Reps.* **2017**, *7*, 13225.

[5] a) Y. Lu, L. Wang, J. Cheng, J. B. Goodenough, *Chem. Commun*. **2012**, *48*, 6544-6546, b) T. Matsuda, M. Takachi, Y. Moritomo, *Chem. Commun*. **2013**, *49*, 2750-2752, c) M. Takachi, T. Matsuda, Y. Moritomo, *Appl. Phys. Express* **2013**, *6*, 025802, d) Y. You, X.-L. Wu, Y.-X. Yin, Y.-G. Guo, *J. Mater. Chem. A*, **2013**, *1,* 14061-14065, e) D. Yang, J. Xu, X.-Z. Liao, Y.-S. He, H. Liu, Z.-F. Ma, *Chem. Commun*. **2014**, *50*, 13377-13380, f) H. W. Lee, R. Y. Wang, M. Pasta, S. W. Lee, N. Liu, Y.Cui, *Nat. Commun*. **2014**, *5*, 5280, g) L. Wang, J. Song, R. Q. Qiao, L. A. Wray, M. A. Hossain, T.-D. Chung, W. Yang, Y. Lu, D. Evans, J,-J, Lee, S. Vail, X. Zhao, M. Nishijima, S. Kakimoto, J. B. Goodenough, *J. Am. Chem. Soc.* **2015**, *137*, 2548-2554, h) S. Yu, Y. Li, Y. Lu, B. Xu, Q. Wang, M. Yan, Y. A. Jiang, *J. Power Sources*, **2015**, *275*, 45-49, i) M. Xie, M. Xu, Y. Huang, R. Chen, X. Zhang, L. Li, F. Wu, *Electrochem. Commun.* **2015**, *59*, 91-94, j) Y. Moritomo, S. Urase, T. Shibata, *Electrochim. Acta* **2016**, *210*, 963-969.

[6] a) C. D. Wessells, S. V. Peddada, R. A. Huggins, Y. Cui, *Nano Lett.* **2011**, *11*, 5421-5425, b) C. D. Wessells, M. T. McDowell, S. V. Peddada, M. Pasta, R. A. Huggins, Y. Cui, *ACS Nano.* **2012**, *6*, 1688-1694, c) X. Wu, Y. Luo, M. Sun, J. Qian, Y. Cao, X. Ai, H. Yang, *Nano Energy* **2015**, *13*, 117-123, d) M. Pasta, R. Y. Wang, R. Ruffo, R. Qiao, H.-W. Lee, B. Shyam, M. Guo, Y. Wang, L. A. Wray, W. Yang, M. F. Toney, Y. Cui, *J. Mater. Chem. A*, **2016**, *4*, 4211-4223, e) K. Nakamoto, R. Sakamoto, M. Ito, A. Kitajou, S. Okada, *Electrochemistry* **2016**, *85*, 179-185, f) W. Li, F. Zhang, X. Xiang, X. Zhang, *J. Phys. Chem. C* **2017**, *121*, 27805-27812.

[7] M. Takachi, T. Matsuda, Y. Moritomo, *Jpn. J. Appl. Phys.* **2013**, *52*, 090202.

[8] F. Nakada, H. Kamioka, Y. Moritomo, J. E. Kim, M. Takata, *Phys. Rev. B* **2008**, *77*, 224436.

[9] T. Shibata, F. Nakada, H. Kamioka, Y. Moritomo, J. Phys. Soc. Jpn. **2008**, *77*, 104714.

[10] R. G. Bates and V. E. Bower, J. Res. Natl. Bur. Stand., **1954**, 53, 283-290.

[11] H. Iwaizumi, Y. Fujiwara, Y. Fukuzumi, Y. Moritomo, *Dalton Trans.* **2019**, *48*, 1964-1968.

Entry for the Table of Contents

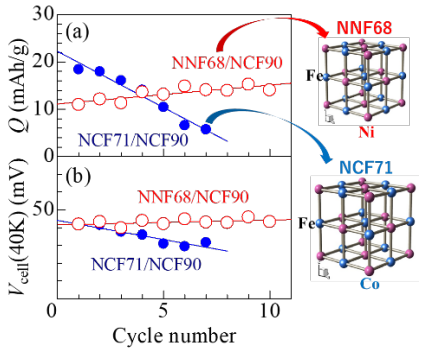

Tertiary battery is charged by the environmental heat and is a promisingenergy harvesting device for the IoT society. The thermal cyclability is not good in the prototypical $Na_xCo[Fe(CN)_6]_{0.71}$ (NCF71)/$Na_xCo[Fe(CN)_6]_{0.90}$ (NCF90) tertiary battery. Here, we significantly improved the thermal cyclability of the tertiary battery with using Ni-substituted $Na_xNi[Fe(CN)_6]_{0.68}$ (NNF68). The improvement is ascribed to poorer crystallinity and smaller unit cell size of the NNF68 film.